

IET Generation, Transmission & Distribution

Special issue Call for Papers



**Be Seen. Be Cited.
Submit your work to a new
IET special issue**

**"Emerging Applications of
IoT and Cybersecurity for
Electrical Power Systems"**

**Lead Guest: Editor Mohamed
M. F. Darwish**




**Guest Editors: Mahmoud
Elsisi, Diao-Eldin A. Mansour,
Mostafa M. Fouda and Matti
Lehtonen**

Read more



ORIGINAL RESEARCH

Proportional-resonant based control strategy for grid-connected packed-E cell inverters with Lyapunov filter-based PLL

Samet Biricik¹  | Hasan Komurcugil²  | Hafiz Ahmed³  | Mohammad Sharifzadeh⁴ | Majid Mehrasa⁵ | Kamal Al-Haddad⁴

¹Department of Electrical and Electronic Engineering, European University of Lefke, Lefke, Turkey

²Department of Computer Engineering, Eastern Mediterranean University (EMU), Famagusta Mersin 10, Turkey

³Nuclear Futures Institute, Bangor University, Bangor, Gwynedd, UK

⁴École de Technologie Supérieure, University of Quebec, Montreal, QC, Canada

⁵Université Grenoble Alpes, G2Elab, Grenoble, France

Correspondence

Hafiz Ahmed, Nuclear Futures Institute, Bangor University, Bangor, Gwynedd LL57 2DG, UK.
Email: hafiz.ahmed@bangor.ac.uk

Funding information

European Regional Development Fund, Grant/Award Number: Ser Cymru II 80761-BU-103

Abstract

A proportional-resonant (PR)-based current control strategy for grid-connected packed-E cell (PEC) inverter is presented. Unlike the existing control strategies, which are based on proportional-integral controller, developed for packed-U cell and PEC inverters, the proposed PR-based control strategy achieves zero steady-state error in the grid current. Furthermore, it eliminates the necessity of employing the control loop for regulating the dc capacitor voltages. Also, the grid current synchronization is achieved by using a Lyapunov filter-based phase locked loop (PLL). The consequence of using Lyapunov filter-based PLL is that sinusoidal synchronization signal can be extracted from the distorted grid voltage. The performances of the proposed control strategy under steady-state, load variation and non-ideal grid voltage are investigated on a laboratory-scale experimental prototype. It is reported that the control of both dc- and ac-side variables of the system are accomplished.

1 | INTRODUCTION

The need for efficient power conversion is essential in grid-connected inverters [1–3]. With the aim of achieving high efficiency in power conversion, multi-level inverters (MIs) [4, 5] have become very popular in the last two decades. The MI topologies include the neutral point clamped (NPC) inverter [6], flying capacitor (FC) inverter [7], cascaded H-bridge inverter [8], T-type inverter [9], and packed-U-cell (PUC) inverter [10]. However, the main drawbacks of NPC, FC and T-type inverters are the difficulty in the implementation and cost due to the high number of switches, capacitors and diodes employed in a typical n-level inverter. For instance, a single-phase grid-connected NPC inverter can generate a five-level quasi-sinusoidal voltage by using eight switches, four diodes and two dc capacitors.

Similarly, a single-phase T-type inverter produces a five-level quasi-sinusoidal voltage by using eight switches and two dc capacitors without using clamping diodes. In addition, the complexity to design an appropriate controller is dramatically

increased [11]. The main reason of this complexity comes from the challenge of voltage balancing of the dc capacitors.

The PUC inverter has recently emerged in MI topology, which has the ability to produce five-level (PUC5) [12], and seven-level (PUC7) quasi-sinusoidal voltages using minimum number of components (six switching devices and one dc capacitor) compared to NPC and T-type topologies [13]. It is worth noting that the five-level voltage can be obtained when the dc capacitor voltage is balanced to the half of input dc voltage. On the other hand, a seven-level voltage can be produced when the dc capacitor voltage is balanced to the one-third of dc input voltage. Owing to the reduced number of switching devices and dc capacitor requirement, the performance of PUC inverters is investigated in various applications such as active filter [14, 15], dynamic voltage restorer [16], rectifier [17, 18], stand-alone inverter [18–21], and grid-connected inverter [20–28].

In the grid-connected mode, the control of both dc capacitor voltage and ac current injected into the grid is essential. In [20], the dc capacitor control is achieved by a sensor-less

This is an open access article under the terms of the [Creative Commons Attribution-NonCommercial-NoDerivs License](https://creativecommons.org/licenses/by-nc-nd/4.0/), which permits use and distribution in any medium, provided the original work is properly cited, the use is non-commercial and no modifications or adaptations are made.

© 2022 The Authors. *IET Generation, Transmission & Distribution* published by John Wiley & Sons Ltd on behalf of The Institution of Engineering and Technology.

control based on redundant switching states which are taken into consideration in the switching process. In this case, the need for measuring the capacitor voltage is eliminated. However, the grid current is controlled by a proportional-integral (PI) controller whose performance is not satisfactory for ac signals. Various model predictive control (MPC) methods are proposed to solve the control problem of grid-connected PUC inverters [22–26]. Although the MPC methods offer some advantages which include easy implementation, good current (or voltage) quality, and low distortion, they suffer from the disadvantages such as sensitivity to parameter variations and weighting factor requirement [22–25]. In [26], a Lyapunov-based MPC is proposed for grid-connected PUC inverters. Although this method eliminates the need for employing weighting factor in the cost function, the parameter sensitivity remains unresolved. The parameter sensitivity problem can be overcome by using sliding mode control [21, 27]. However, sliding mode control suffers from chattering which leads time-varying switching frequency. Time-varying switching frequency is not desired in practice. Even though the control methods mentioned so far offer various advantages and disadvantages regarding the steady-state and dynamic performances of the system, regulation of dc capacitor voltages becomes challenging when the seven-level PUC inverter is extended to nine-level PUC inverter (PUC9). The main reason of this comes from the fact that the design of PUC7 topology was based on employing six switching devices and one dc capacitor whose voltage should be adjusted to one-third of the input dc voltage. Extension to nine-level increases the number of switching devices from six to eight and dc capacitors from one to two which increases the controller complexity considerably [28, 29].

As an alternative to PUC9, packed-E cell (PEC) inverter is introduced in [30]. The structure of PEC topology involves six switching devices, one back-to-back bidirectional switching device and two dc capacitors. Unlike the PUC9 topology, the voltage regulation of dc capacitors can be achieved easily in PEC inverter topology. In this topology, the capacitor voltages are regulated to half of input dc voltage. The main reason of this voltage regulation easiness is due to the use of E-cell in which both capacitors are charged and discharged simultaneously. As a consequence of simultaneous charging/discharging, both capacitors have equal voltage which causes equal voltage stress on both capacitors. This feature makes PEC topology one step ahead of the PUC9 topology in which the capacitor voltages are not equal. In [30], the capacitor voltages are regulated by an active balancing algorithm which is integrated into the half parabola carrier PWM. In [31], a modified level shifted PWM technique is proposed for balancing capacitor voltages. However, in these studies, the PEC inverter is operated in the standalone mode only. To the best of author's knowledge, the performance of PEC inverter in the grid-connected mode is investigated only in [32]. The control method is based on sliding mode control which is optimized by artificial bee colony algorithm. Even though the steady-state and dynamic responses are satisfactory, the performance of the system under distorted grid is not studied. Furthermore, the sliding mode control is subject to chattering which causes high frequency in the vicinity of

sliding surface. In order to alleviate the effect of chattering, the sign function is replaced by saturation function. However, this leads to steady-state error in the grid-current. In [33], a finite set MPC (FS-MPC) is proposed. However, FS-MPC is sensitive to parameter variations. Also, the switching frequency is time-varying. In [34], a feedback linearization with artificial neural network (ANN) is proposed. However, this control method employs six control gains whose tuning is very complicated. Also, a dq transformation is essential which complicates the design of the method in practice.

The existing control strategies devoted for PUC inverters are generally based on using two proportional-integral (PI) controllers which control the dc- and ac-side variables [10, 13, 14]. However, the performance of PI controller in controlling dc quantities is not satisfactory since it cannot guarantee zero steady-state error [20, 35]. PR controller can track the ac signal with zero steady-state error thanks to the theoretically infinite gain at the fundamental frequency. Furthermore, the performance of grid-connected inverter under distorted grid is not studied. Here, proportional-resonant (PR)-based control strategy is proposed for a grid-connected nine-level PEC (PEC9) inverter. Unlike the existing control methods which employ PI controller in the grid current control, the proposed control approach employs a PR controller for achieving the grid current control. The grid current tracking error is passed through the PR controller, which generates a sinusoidal modulating signal. Thereafter, the modulating signal is utilized to generate the PWM signals. In addition to this, Lyapunov filter-based PLL is used to achieve the grid current synchronization with the grid voltage under undistorted as well as distorted grid conditions. The Lyapunov's theorem is also very useful in controlling various power converters [36–38]. The performance of the system is tested by experimental studies.

This paper is organized as follows. In Section 2, the packed E-cell inverter and its operation in the grid-connected mode is explained. In Section 3, the proposed control strategy as well as the proposed Lyapunov-estimator-based synchronization method are introduced. In Section 4, the experimental results obtained for the steady-state, load variation and distorted grid voltage condition are presented with relevant discussions. Finally, Section 5 derives some conclusions.

2 | GRID-CONNECTED PACKED E-CELL INVERTER

Packed E-Cell (PEC) multi-level inverter is developed by improving another existing multi-level inverter, which is the Packed U-Cell (PUC) [39] inverter. PEC is compromised topology between half-bridge and E-Cell type of switch-capacitor connection which totally includes six active power switches and the backed-to-backed connected switches as one bidirectional switch. PEC idea emerged by replacing U-Cell by E-Cell to horizontally extend the capacitors and to make single auxiliary dc-link, while PUC vertically develops the capacitors that creates several separated auxiliary dc-link. As a result of the horizontal extension of capacitors, they would be

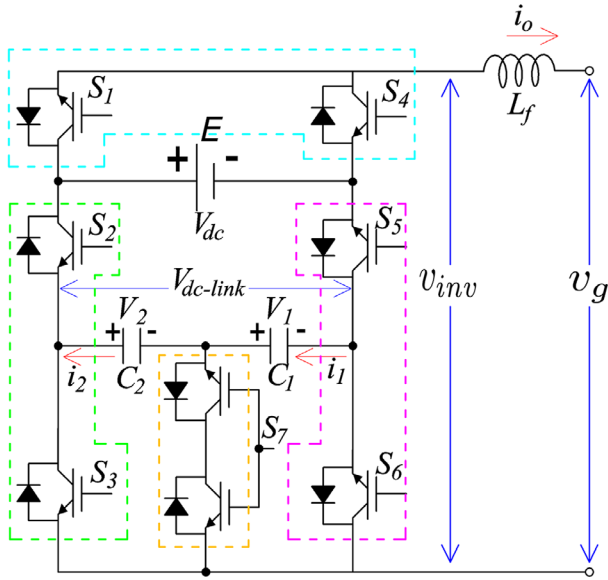


FIGURE 1 The schematic diagram of the grid-connected PEC9 inverter

in harmony of charging and discharging with redundant states that can be effectively used to guarantee the active capacitor voltage balancing. Therefore, PEC topology has reduced the component count and the auxiliary dc-link in comparison to PUC topology. The grid-connected PEC inverter is shown in Figure 1.

With correct switching states sequence operation, PEC configuration can generate nine-level voltage waveform provided that the capacitor voltages are balanced to the quarter of the input dc voltage. Table 1 shows 24 switching states of the 9-level packed E-Cell (PEC9) configured as grid-connected inverter. It can be shown from Table 1 that both capacitors are charged (or discharged) simultaneously during the switching states which produce the middle voltage level ($\pm E/2$). This means that the remaining switching states are not effective in charging (or discharging) these dc capacitors. If the voltage across auxiliary dc-link is regulated to half of the input dc voltage using the corresponding redundant states, both capacitors are inherently balanced to the quarter of same voltage amplitude. Therefore, the capacitor voltages are no longer required to be considered in grid-connected dynamical equations which will simplify designing the final controller. The PEC topology has six switching devices (S_1, S_2, S_3, S_4, S_5 , and S_6) and one cascaded switch S_7 which are supported with a single dc source and two capacitors (C_1 and C_2). With the proper switching selection, a nine-level voltage waveform can be achieved at the inverter terminals (v_{inv}). Switching states of PEC9 are given in Table 1.

3 | PROPOSED CONTROL STRATEGY

The proposed control strategy should be able to work under ideal and distorted grid voltage conditions. Therefore, first, grid synchronization using Lyapunov estimator approach is discussed. Then, the proposed control strategy is introduced.

3.1 | Grid synchronization using Lyapunov estimator

Single-phase grid voltage signal can be expressed as,

$$\begin{aligned} v_g(t) &= V_g(t) \sin \{ \omega t + \phi(t) \}, \\ &= V_g(t) \{ \sin(\omega t) \cos(\phi(t)) + \cos(\omega t) \sin(\phi(t)) \}, \\ &= V_g(t) \sin(\phi(t)) \cos(\omega t) + V_g(t) \cos(\phi) \sin(\omega t), \end{aligned} \quad (1)$$

where ω is the angular frequency with the nominal value $\omega_n = 2\pi f$ and the instantaneous phase is given by $\varphi = \omega t + \phi$. For further development, time-dependence of a signal is often not explicitly stated for convenience. Now, let us assume $\theta = [\theta_1 \ \theta_2]^T$ with $\theta_1 = V_g \sin(\phi)$, $\theta_2 = V_g \cos(\phi)$ and $\mathbf{x} = [\cos(\omega t) \ \sin(\omega t)]^T$. Then, the measured grid voltage signal in parametric form can be written as [40–43]:

$$\begin{aligned} v_g &= \underbrace{[V_g \sin(\phi) \ V_g \cos(\phi)]}_{\theta^T} \underbrace{[\cos(\omega t) \ \sin(\omega t)]^T}_{\mathbf{x}}, \\ &= \theta^T \mathbf{x}. \end{aligned} \quad (2)$$

Equation (2) assumes that the grid frequency (f) is constant at 50 or 60 Hz. However, grid frequency may vary due to many reasons. To overcome this issue, a frequency estimator is also designed in this work. Then, the problem considered in this work is to estimate the varying parameter vector θ from the measurement $v_g(t)$ and the known information vector \mathbf{x} . For this purpose, Lyapunov estimator will be considered. To design the Lyapunov estimator, let us consider that the estimation error as:

$$\begin{aligned} v_e &= v_g - \hat{v}_g, \\ &= \theta^T \mathbf{x} - \hat{\theta}^T \mathbf{x}, \\ &= (\theta^T - \hat{\theta}^T) \mathbf{x}, \\ &= \tilde{\theta}^T \mathbf{x}, \end{aligned} \quad (3)$$

where $\hat{\cdot}$ indicates estimated value and $\tilde{\theta} = \theta - \hat{\theta}$. Then, the following Lyapunov-like function has been considered:

$$V(\tilde{\theta}) = \frac{\tilde{\theta}^T \Omega^{-1} \tilde{\theta}}{2}, \quad (4)$$

where $\Omega = \Omega^T > 0$ with $\Omega = \zeta I_2$, $\zeta > 0$ and I_2 is the identity matrix of dimension 2×2 . From (4), one can obtain

$$\begin{aligned} \dot{V}(\tilde{\theta}) &= \frac{1}{2} \left\{ (\dot{\tilde{\theta}})^T \Omega^{-1} \tilde{\theta} + \tilde{\theta}^T \Omega^{-1} \dot{\tilde{\theta}} \right\}, \\ &= \tilde{\theta}^T \Omega^{-1} \dot{\tilde{\theta}}, \end{aligned}$$

TABLE 1 Switching states table of PEC9 inverter [30]

State number	Switching states							dc Side		ac Side		
	1	2	3	4	5	6	7	V_1	V_2	i_0	v_{inv}	
1	1	0	0	0	1	1	0	—	—	Positive half cycle	+	$V_{dc} = +E$
2	1	0	0	0	1	0	1	↓	—		+	$V_{dc} - V_1 = +3E/4$
3	1	0	1	0	1	0	0	↓	↓		+	$V_{dc} - V_1 - V_2 = +E/2$
4	1	1	0	0	0	1	0	↑	↑		+	$V_1 + V_2 = +E/2$
5	1	1	0	0	0	0	1	—	↑		+	$V_2 = +E/4$
6	0	0	0	1	1	1	0	—	—		+	0
7	1	1	1	0	0	0	0	—	—		+	0
8	0	0	0	1	1	0	1	↓	—		+	$-V_1 = -E/4$
9	0	1	0	1	0	1	0	↑	↑		+	$-V_{dc} + V_1 + V_2 = -E/2$
10	0	0	1	1	1	0	0	↓	↓		+	$-V_1 - V_2 = -E/2$
11	0	1	0	1	0	0	1	—	↑		+	$-V_{dc} + V_2 = -3E/4$
12	0	1	1	1	0	0	0	—	—		+	$V_{dc} = -E$
13	1	0	0	0	1	1	0	—	—	Negative half cycle	—	$V_{dc} = +E$
14	1	0	0	0	1	0	1	↑	—		—	$V_{dc} - V_1 = +3E/4$
15	1	0	1	0	1	0	0	↑	↑		—	$V_{dc} - V_1 - V_2 = +E/2$
16	1	1	0	0	0	1	0	↓	↓		—	$V_1 + V_2 = +E/2$
17	1	1	0	0	0	0	1	—	↓		—	$V_2 = +E/4$
18	0	0	0	1	1	1	0	—	—		—	0
19	1	1	1	0	0	0	0	—	—		—	0
20	0	0	0	1	1	0	1	↑	—		—	$-V_1 = -E/4$
21	0	1	0	1	0	1	0	↓	↓		—	$-V_{dc} + V_1 - V_2 = -E/2$
22	0	0	1	1	1	0	0	↑	↑		—	$-V_1 - V_2 = -E/2$
23	0	1	0	1	0	0	1	—	↓		—	$-V_{dc} + V_2 = -3E/4$
24	0	1	1	1	0	0	0	—	—		—	$V_{dc} = -E$

$$\begin{aligned}
&= \tilde{\theta}^T \Omega^{-1} (\dot{\theta} - \hat{\dot{\theta}}), \\
&= -\tilde{\theta}^T \Omega^{-1} \hat{\dot{\theta}},
\end{aligned} \tag{5}$$

where we assumed that the parameters are constant and/or slowly varying, that is, $\dot{\theta} = 0$. If the parameter update law is selected as:

$$\dot{\hat{\theta}} = \Omega \mathbf{x} v_e. \tag{6}$$

Then, the derivative of the Lyapunov-like function becomes:

$$\begin{aligned}
\dot{V}(\tilde{\theta}) &= -\tilde{\theta}^T \Omega^{-1} \Omega \mathbf{x} v_e, \\
&= -\tilde{\theta}^T \mathbf{x} v_e, \\
&= -v_e v_e, \\
&= -v_e^2 \leq 0.
\end{aligned} \tag{7}$$

As a result, boundedness of the parameter estimation error can be easily established. Since the information vector \mathbf{x} is sufficiently rich (i.e. persistently exciting), the convergence of the parameter vector can be easily established through the Theorem presented in [44]. Estimator (6) in terms of individual parameters are given below:

$$\dot{\hat{\theta}}_1 = \zeta \cos(\omega t) (v_g - \hat{v}_g), \tag{8}$$

$$\dot{\hat{\theta}}_2 = \zeta \sin(\omega t) (v_g - \hat{v}_g), \tag{9}$$

$$\hat{v}_g = [\cos(\omega t) \quad \sin(\omega t)] [\hat{\theta}_1 \quad \hat{\theta}_2]^T. \tag{10}$$

It is to be noted here that in our case $\hat{\omega}$ will be used instead of ω as the grid frequency may fluctuate. From the estimated parameter vector $\hat{\theta}$, the grid voltage amplitude and phase angle can be estimated as:

$$\hat{\phi} = \text{atan2}(\hat{\theta}_1, \hat{\theta}_2), \tag{11}$$

$$\hat{V}_g = \sqrt{\hat{\theta}_1^2 + \hat{\theta}_2^2}. \tag{12}$$

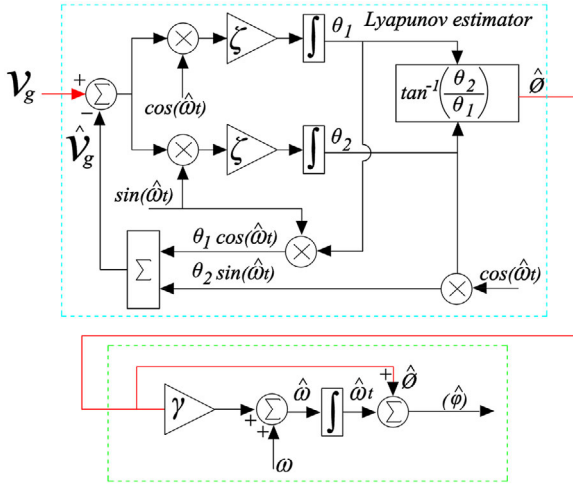


FIGURE 2 Lyapunov filter-based PLL configuration, where $\gamma > 0$ is the frequency estimation gain

From the estimated phase angle $\hat{\phi}$, the instantaneous frequency can be easily estimated by using some additional mathematical manipulation. Finally, the filtered grid frequency can be rewritten as:

$$\hat{v}_g(t) = V_g(t) \sin \{ \hat{\omega}t + \hat{\phi}(t) \}. \quad (13)$$

The complete block diagram of Lyapunov filter-based PLL is depicted in Figure 2.

To tune the proposed PLL, small-signal modelling can be used. In [45], it has been found that the Lyapunov estimator tuning gain ζ can be tuned as: $\zeta = 8/t_{ss}$, where t_{ss} is the desired settling time. Then, applying the small-signal PLL model given in [46] to the developed PLL in this work, the frequency estimation gain γ can be tuned as a function of the phase margin and/or settling time.

3.2 | Proportional resonant current controller

The use of PR controller guarantees zero tracking error of the ac signals in the steady-state. Hence, the control of grid current can be achieved by a PR controller whose transfer function is given by [47–50]:

$$G_{PR}(s) = K_p + \frac{2K_r\omega_c s}{s^2 + 2\omega_c s + \omega^2}, \quad (14)$$

where ω_c denotes the cut-off frequency, ω denotes the resonant frequency, and K_p and K_r are the proportional and resonant gains, respectively. The input applied to the PR controller is the grid current error ($i_o^* - i_o$). The PR controller responds to this input by producing a modulating signal which is needed in generating the PWM signals by comparing it with the triangular carrier signals. With respect to the current controller, the transfer function $G_{PR}(s)$ can be written as: $G_{PR}(s) = M(s)/X(s)$, where $X(s)$ denotes the grid current tracking error ($i_o - i_o^*$) and $M(s)$ is the modulating signal in Laplace domains, respectively.

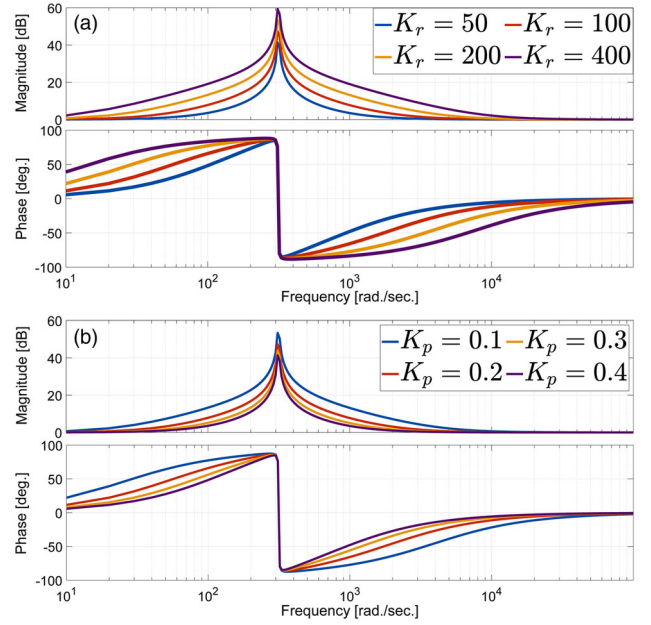


FIGURE 3 Bode diagram of $G_{PR}(s)$ by using different K_p and K_r values. (a) $K_p = 0.1$ and varying K_r , (b) $K_r = 200$ and varying K_p

The main goal behind PR controller is based on having a sharp peak in the magnitude response of $G_{PR}(s)$ which is located at ω . Hence, if ω is set to the frequency of i_o^* , which is 100π rad/s in this study, then a sinusoidal modulating signal is generated at the output of PR. In such a case, the grid current will be controlled and zero steady-state error in the grid current will be attained. The Bode plot of $G_{PR}(s)$ has been plotted by using different K_p and K_r values and given in Figure 3. In Figure 3a, the magnitude and phase responses of $G_{PR}(s)$ are plotted by using different K_r values while K_p is fixed at 0.1. It can be seen from the magnitude response that $G_{PR}(s)$ has a peak located at $\omega = 100\pi$ rad/s. The width of this peak can be adjusted by varying K_r . When K_r is decreased, the peak becomes narrower which in turn reduces the steady-state error in the grid current. Contrary to K_r , the peak becomes wider when K_p is decreased while K_r is constant, as shown in Figure 3b. Since there is no analytical formula to compute the values of K_p and K_r , they should be selected based on the desired performance of the inverter. It is to be noted here that for real-time implementation, PR controller (14) needs to be discretized. In the literature, Tustin method has been widely used to discretize the continuous-time PR controller [48]. The same approach has been considered here. The discretized PR controller equations are avoided here as they are widely available in the literature.

The reference of grid current is given by:

$$i_o^* = I_o^* \sin(\hat{\phi}), \quad (15)$$

where I_o^* denotes amplitude of reference grid current i_o^* . The proposed control approach is different from the existing control strategies which are generally based on using two proportional-integral (PI) controllers which control the dc- and ac-side variables [10, 13, 14], but the performance of PI controller in

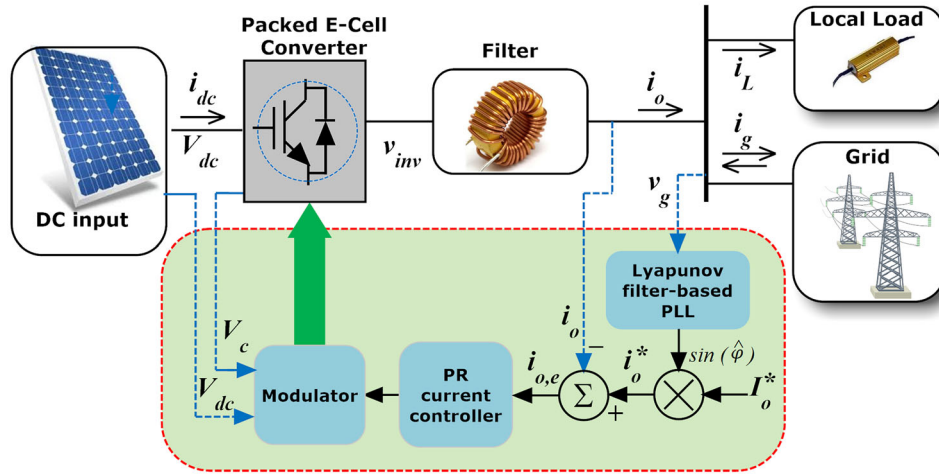


FIGURE 4 Block diagram of the proposed control strategy together with the grid-connected PEC9 inverter

controlling dc quantities is not satisfactory since it cannot guarantee zero steady-state error [20]. When the grid current tracks its reference with zero steady-state error, then the capacitor voltages are controlled indirectly. Hence, there is no need to employ controller to adjust the dc capacitor voltages.

4 | EXPERIMENTAL RESULTS AND DISCUSSION OF THE PROPOSED PR-BASED CONTROL TECHNIQUE

In this section, the experimental analysis is done to confirm the feasibility of the proposed PR-based control strategy using the prototype of a grid-connected PEC9 inverter which is built by the switches type of C3M0120090D. The complete control block diagram of the system is shown in Figure 4, where V_c is the series-connected capacitor voltage.

Thanks to the hardware controller dSPACE 1104, the designed PR-based controller has been successfully implemented to control the PEC9 switches with associated I/Os. The high voltage/current OPAL-RT measurement is also utilized to measure the grid voltage, inverter current, auxiliary and main dc voltages to reduce their amplitude to the safe range which can be sent to the dSPACE 1104 ADC ports. The whole experimental setup test with all details is shown in Figure 5.

Also, the system and control parameters which are used in the experimental tests are provided in Table 2. The performance of proposed PR-based controller has been investigated under different operational conditions such as steady and dynamic states, load variations, ideal and non-ideal grid voltages.

4.1 | Steady-state performance test

In this section, the proposed PR-based controller for the grid-connected PEC9 inverter has been tested under steady-state operation. Figure 6 shows the steady-state responses of V_c , v_{inv} , v_g and i_o for $I_o^* = 4$ A.

TABLE 2 System and control parameters

Grid voltage amplitude, V_g	130V (peak)
Grid impedance, Z_g	0.1 Ω and 2.5mH
Grid frequency, f	50Hz
dc voltage, V_{dc}	160V
Auxiliary dc link capacitors (C1 & C2)	2500 μ F (each)
Filter inductance, L_f	2.5mH
Load 1 impedance, R_{L1}	40 Ω
Load 2 impedance, R_{L2}	40 Ω
Lyapunov estimator parameters (ζ, γ)	(250, 50)

It can be seen from Figure 6 that the voltage across the series-connected capacitors (V_c) is regulated using the redundant switching states of Table 1 at 80 V, which is half of V_{dc} and consequently the capacitor voltages (V_1 and V_2) are self-adjusted at 40 V. The inverter voltage (v_{inv}) has the perfect nine levels which are consistent with the values in Table 1. The grid current (i_o) that has 4 A amplitude is sinusoidal waveform, which is in phase with the grid voltage (v_g). This implies that the proposed Lyapunov-based PLL works correctly. Also, the proposed current control strategy is able to inject the desired current into the grid side. Figure 7 shows spectrums of grid voltage and grid current that correspond to Figure 6.

The total harmonic distortions (THDs) of the grid voltage and grid current are measured as 1.1% and 2.8%, respectively, which indicate that the distortion of the grid current is below IEEE Std. 1250-2018.

4.2 | Performance test under load variations

The performance of the proposed PR-based control strategy is also tested under load variations. Figure 8 shows the responses of dc- and ac-side variables of the grid-connected PEC9 inverter for a step change in I_o^* from 8 to 4 A.

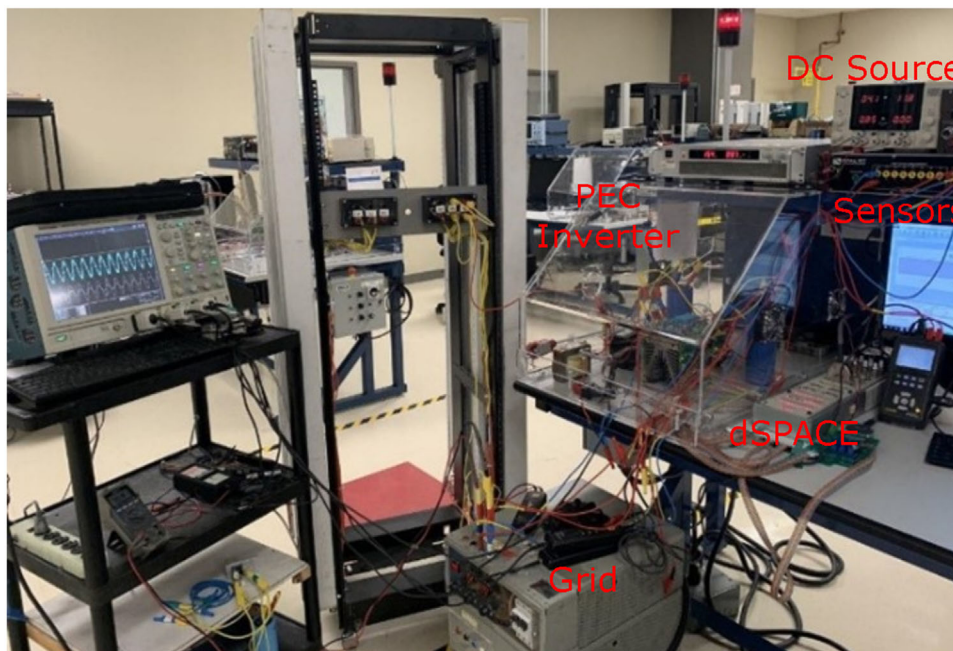


FIGURE 5 Experimental test setup of the grid-connected PEC9 inverter

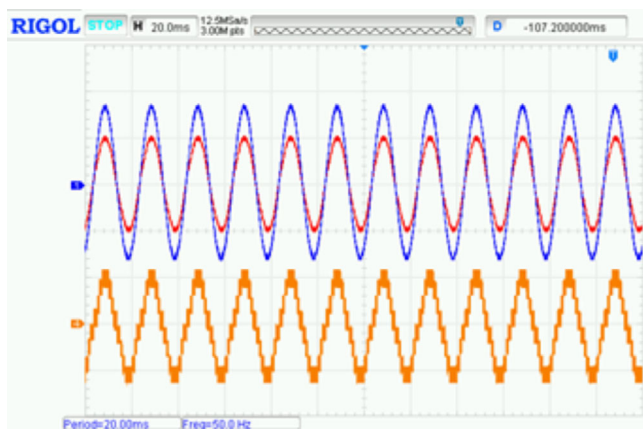


FIGURE 6 Steady-state responses of dc- and ac-side variables of the grid-connected PEC9 inverter for $I_o^* = 4$ A. (V_c : 40 V/div, v_{im} : 80 V/div, v_g : 100 V/div, i_o : 10 A/div)

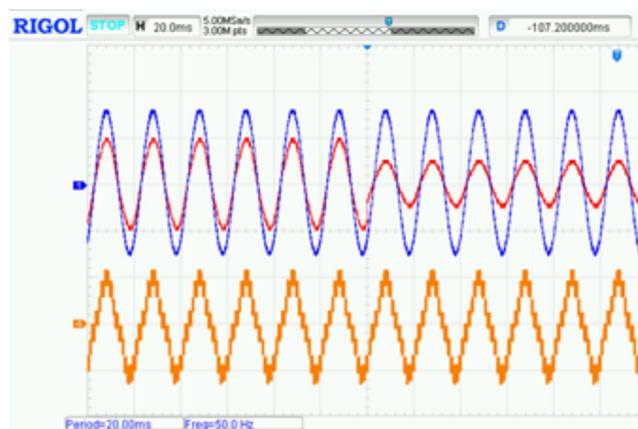


FIGURE 8 Responses of dc- and ac-side variables of the grid-connected PEC9 inverter for a step change in I_o^* from 8 to 4 A, (V_c : 40 V/div; v_{im} : 80 V/div; v_g : 100 V/div; i_o : 10 A/div)

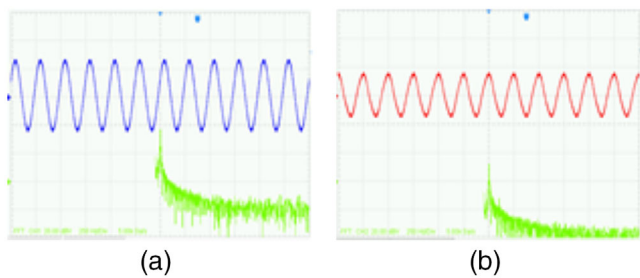


FIGURE 7 Frequency spectrum of grid voltage and grid current in Figure 6. (a) Grid voltage; (b) grid current

The step change in the current occurs when the load connected to the inverter is changed from 40 to 80 Ω . It is evident that the dc voltage across the series-connected capacitors is not

affected by this step change in the reference grid current amplitude. The inverter output voltage is not distorted except for the short transient period and has nine levels in accordance with the values given in Table 1. It is obvious that the grid current has sinusoidal waveform and it is in phase with the grid voltage before and after the current change. Even though the reference grid current and grid current error are not shown in Figure 8, it can be concluded that the PR-based control strategy guarantees zero steady-state error in the grid current and fast dynamic response in tracking the reference grid current.

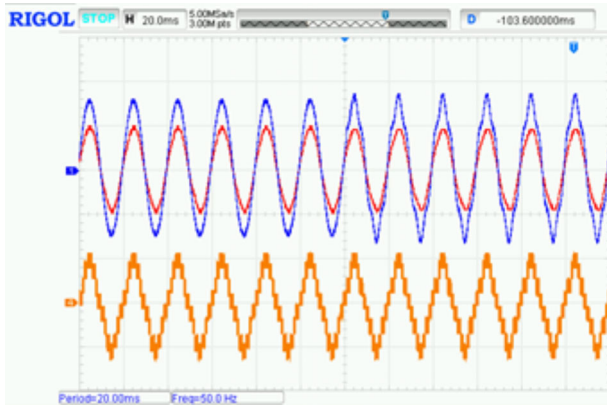


FIGURE 9 Responses of and ac-side variables of the grid-connected PEC9 inverter when the grid voltage is changed from ideal to non-ideal, (V_c : 40 V/div, v_{inv} : 80 V/div, v_g : 100 V/div, i_o : 10 A/div)

4.3 | Performance test under non-ideal grid voltage

The performance of the proposed control strategy is also tested under non-ideal grid voltage condition. Figure 9 shows the responses of dc- and ac-side variables when the grid voltage is changed from ideal to non-ideal condition.

Clearly, dc- and ac-sides variables (V_c , v_{inv} , v_g and i_o) under ideal grid voltage satisfy the control objectives such as the regulation of V_c and control of i_o . When the grid voltage is non-ideal, the Lyapunov filter-based PLL produces ideal sinusoidal signal which is used to synchronize the grid current with grid voltage. During non-ideal grid voltage, the voltage across series-connected capacitors is maintained at 80 V, and the grid current is sinusoidal and in phase with the grid voltage. Also, the inverter voltage produces the perfect nine levels under non-ideal grid voltage condition. Figure 10 shows the harmonic spectrum of non-ideal grid voltage in Figure 9 that the THD of grid voltage is measured to be 3.6%.

The comparison of the existing control methods developed for PEC inverter with the proposed control method is presented

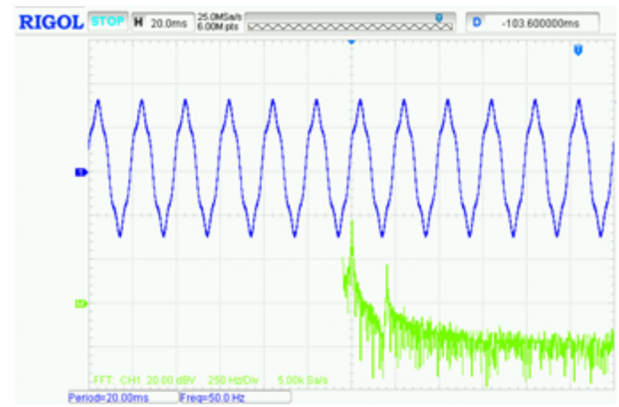


FIGURE 10 Frequency spectrum of grid voltage in Figure 9

as shown in Table 3. It is obvious that the proposed method is more beneficial in terms of dc capacitor voltage control, number of control gains, and steady-state error in the grid current.

5 | CONCLUSION

In this study, a proportional-resonant (PR)-based current control strategy for grid-connected PEC inverter with Lyapunov filter-based PLL is proposed. It is pointed out that the existing control strategies employ PI controller in the grid current loop, which leads to steady-state error. The proposed PR-based control strategy yields zero steady-state error in the grid current. Furthermore, the necessity of employing the control loop for regulating the dc capacitor voltages is eliminated. In addition, Lyapunov filter-based PLL is used to achieve the grid current synchronization under ideal as well as non-ideal grid voltages. The experimental results obtained from the prototype of PEC9 inverter show that the proposed control strategy offers good steady-state and dynamic responses not only under ideal grid voltage, but also under non-ideal grid voltage. The experimental results confirmed the potential of PEC converter. Therefore,

TABLE 3 Comparison of existing control methods with the proposed control method

Comparison category	[30]	[31]	[32]	[33]	[34]	Proposed Method
Operation mode	Standalone	Standalone	Grid-connected	Grid-connected	Grid-connected	Grid-connected
Control method	Not reported	Not reported	Sliding-mode Control	Finite-set MPC	Feedback-linearization and ANN	Proportional Resonant
Dc capacitor voltages control technique	Half-parabola based PWM	Level shifted PWM	Level shifted PWM	Not reported	Not reported	Dedicated switching states
Number of control gains	Not applicable	Not applicable	2	3	6	2
Steady-state error in grid current	Not applicable	Not applicable	Not zero	Not guaranteed to be zero	Guaranteed to be zero	Guaranteed to be zero
Advantages and/or Disadvantages of control method	Not applicable	Not applicable	Chattering, sensitive to parameter variations and variable switching frequency	Sensitive to parameter variations and variable switching frequency	Complicated gain tuning, requires dq transformation and too many computations	Insensitive to parameter variations, zero steady-state error and fixed switching frequency

the employment of PEC converter in power quality issue can be considered as the next future direction.

AUTHOR CONTRIBUTIONS

Samet Biricik: Conceptualization, formal analysis, methodology, software, validation, writing - original draft, writing - review and editing. Hasan Komurcugil: Conceptualization, formal analysis, investigation, methodology, supervision, writing - original draft, writing - review and editing. Hafiz Ahmed: Conceptualization, formal analysis, investigation, methodology, software, validation, visualization, writing - original draft, writing - review and editing. Mohammad Sharifzadeh: Investigation, software, validation, visualization, writing - original draft, writing - review and editing. Majid Mehra: Investigation, software, validation, visualization, writing - original draft, writing - review and editing. Kamal Al-Haddad: Conceptualization, supervision, writing - review and editing.

ACKNOWLEDGEMENT

The work of H. Ahmed is funded through the Sêr Cymru II 80761-BU-103 project by Welsh European Funding Office (WEFO) under the European Regional Development Fund (ERDF).

CONFLICT OF INTEREST

The authors have declared no conflict of interest.

DATA AVAILABILITY STATEMENT

The data that support the findings of this study are available from the corresponding author upon reasonable request.

ORCID

Samet Biricik  <https://orcid.org/0000-0002-1559-2024>

Hasan Komurcugil  <https://orcid.org/0000-0003-4728-6416>

Hafiz Ahmed  <https://orcid.org/0000-0001-8952-4190>

REFERENCES

- Palaniappan, R., Molodchik, O., Shariati-Sarcheshmeh, M., Asmah, M.W., Liu, J., Schlichtherle, T., et al.: Experimental verification of smart grid control functions on international grids using a real-time simulator. *IET Gener. Transm. Distrib.* 16(13), 2747–2760 (2022)
- Kordkandi, R.D., Hagh, M.T., Roozbehani, S.: Real-time low/high-voltage ride-through capability improvement of micro-grid based on coordinated robust grid-following control. *IET Gener. Transm. Distrib.* 16(16), 3318–3332 (2022)
- Ahmed, H., Biricik, S., Benbouzid, M.: A Quasi open-loop robust three-phase grid-synchronization technique for non-ideal grid. *IET Gener. Transm. Distrib.* 15(24), 3388–3399 (2021)
- Alatai, S., Salem, M., Ishak, D., Das, H.S., Alhuyi Nazari, M., Bughneda, A., et al.: A review on state-of-the-art power converters: bidirectional, resonant, multilevel converters and their derivatives. *Appl. Sci.* 11(21), 10172 (2021)
- Ramli, Z., Jamaludin, J., Abd Rahim, N., Azzuhri, S.R.: Capacitor voltage balancing with online controller performance-based tuning for a switching-based multilevel inverter. *Appl. Sci.* 11(10), 4428 (2021)
- Rodriguez, J., Bernet, S., Steimer, P.K., Lizama, I.E.: A survey on neutral-point-clamped inverters. *IEEE Trans. Ind. Electron.* 57(7), 2219–2230 (2010)
- Feng, C., Liang, J., Agelidis, V.G.: Modified phase-shifted PWM control for flying capacitor multilevel converters. *IEEE Trans. Power Electron.* 22(1), 178–185 (2007)
- Zhao, T., Zhang, X., Mao, W., Wang, F., Xu, J., Gu, Y., et al.: An optimized third harmonic compensation strategy for single-phase cascaded H-bridge photovoltaic inverter. *IEEE Trans. Ind. Electron.* 65(11), 8635–8645 (2018)
- Shao, Z., Zhang, X., Wang, F., Cao, R.: Modeling and elimination of zero-sequence circulating currents in parallel three-level T-type grid-connected inverters. *IEEE Trans. Power Electron.* 30(2), 1050–1063 (2015)
- Ounejar, Y., Al-Haddad, K., Gregoire, L.A.: Packed U cells multilevel converter topology: theoretical study and experimental validation. *IEEE Trans. Ind. Electron.* 58(4), 1294–1306 (2011)
- Rodriguez, J., Bernet, S., Wu, B., Pontt, J.O., Kouro, S.: Multilevel voltage-source-converter topologies for industrial medium-voltage drives. *IEEE Trans. Ind. Electron.* 54(6), 2930–2945 (2007)
- Sharifzadeh, M., Vahedi, H., Al-Haddad, K.: New constraint in SHE-PWM for single-phase inverter applications. *IEEE Trans. Ind. Appl.* 54(5), 4554–4562 (2018)
- Vahedi, H., Al-Haddad, K.: Real-time implementation of a seven-level packed U-cell inverter with a low-switching-frequency voltage regulator. *IEEE Trans. Power Electron.* 31(8), 5967–5973 (2016)
- Vahedi, H., Shojaei, A.A., Dessaint, L.A., Al-Haddad, K.: Reduced DC-link voltage active power filter using modified PUC5 converter. *IEEE Trans. Power Electron.* 33(2), 943–947 (2018)
- Sahli, A., Krim, F., Laib, A., Talbi, B.: Energy management and power quality enhancement in grid-tied single-phase PV system using modified PUC converter. *IET Renewable Power Gener.* 13(14), 2512–2521 (2019)
- Trabelsi, M., Komurcugil, H., Refaat, S.S., Abu-Rub, H.: Model predictive control of packed U cells based transformerless single-phase dynamic voltage restorer. In: 2018 IEEE International Conference on Industrial Technology (ICIT), pp. 1926–1931. IEEE, Piscataway, NJ (2018)
- Makhamreh, H., Trabelsi, M., Kükrer, O., Abu-Rub, H.: A Lyapunov-based model predictive control design with reduced sensors for a PUC7 rectifier. *IEEE Trans. Ind. Electron.* 68(2), 1139–1147 (2021)
- Ounejar, Y., Al-Haddad, K., Dessaint, L.A.: A novel six-band hysteresis control for the packed U cells seven-level converter: experimental validation. *IEEE Trans. Ind. Electron.* 59(10), 3808–3816 (2012)
- Biricik, S., Komurcugil, H.: Proportional-integral and proportional-resonant based control strategy for PUC inverters. In: IECON 2018-44th Annual Conference of the IEEE Industrial Electronics Society, pp. 3369–3373. IEEE, Piscataway, NJ (2018)
- Vahedi, H., Labbé, P.A., Al-Haddad, K.: Sensor-less five-level packed U-Cell (PUC5) inverter operating in stand-alone and grid-connected modes. *IEEE Trans. Ind. Inf.* 12(1), 361–370 (2016)
- Babaie, M., Sharifzadeh, M., Kanaan, H.Y., Al-Haddad, K.: Switching-based optimized sliding-mode control for capacitor self-voltage balancing operation of seven-level PUC inverter. *IEEE Trans. Ind. Electron.* 68(4), 3044–3057 (2021)
- Trabelsi, M., Bayhan, S., Ghazi, K.A., Abu-Rub, H., Ben-Brahim, L.: Finite-control-set model predictive control for grid-connected packed-U-cells multilevel inverter. *IEEE Trans. Ind. Electron.* 63(11), 7286–7295 (2016)
- Metri, J.I., Vahedi, H., Kanaan, H.Y., Al-Haddad, K.: Real-time implementation of model-predictive control on seven-level packed U-cell inverter. *IEEE Trans. Ind. Electron.* 63(7), 4180–4186 (2016)
- Pahnehkolaei, S.M.A., Vahedi, H., Alfi, A., Al-Haddad, K.: Comparative study of multi-objective finite set predictive control methods with new max-min strategy applied on a seven-level packed U-cell inverter. *IET Power Electron.* 12(9), 2170–2178 (2019)
- Sebaaly, F., Vahedi, H., Kanaan, H.Y., Al-Haddad, K.: Experimental design of fixed switching frequency model predictive control for sensorless five-level packed U-cell inverter. *IEEE Trans. Ind. Electron.* 66(5), 3427–3434 (2019)

26. Makhamreh, H., Sleiman, M., Kükrer, O., Al-Haddad, K.: Lyapunov-based model predictive control of a PUC7 grid-connected multilevel inverter. *IEEE Trans. Ind. Electron.* 66(9), 7012–7021 (2019)
27. Makhamreh, H., Trabelsi, M., Kükrer, O., Abu-Rub, H.: An effective sliding mode control design for a grid-connected PUC7 multilevel inverter. *IEEE Trans. Ind. Electron.* 67(5), 3717–3725 (2020)
28. Babaie, M., Sharifzadeh, M., Al-Haddad, K.: Adaptive ANN based single PI controller for nine-level PUC inverter. In: 2019 IEEE Electrical Power and Energy Conference (EPEC), pp. 1–6. IEEE, Piscataway, NJ (2019)
29. Noghani, K.A., Sharifzadeh, M., Ounejjar, Y., Al-Haddad, K.: Current based model predictive control for DC capacitor optimization in grid-connected and stand-alone nine-level packed U-cell inverter. In: 2019 IEEE 28th International Symposium on Industrial Electronics (ISIE), pp. 787–792. IEEE, Piscataway, NJ (2019)
30. Sharifzadeh, M., Al-Haddad, K.: Packed E-Cell (PEC) converter topology operation and experimental validation. *IEEE Access* 7, 93049–93061 (2019)
31. Ahmadijokani, M., Sharifzadeh, M., Mehrasa, M., Sebaaly, F., Al-Haddad, K.: Modified level-shifted PWM technique with active DC capacitors voltages balancing for nine-level packed E-Cell (PEC9) inverter. In: 2020 IEEE International Conference on Industrial Technology (ICIT), pp. 843–848. IEEE, Piscataway, NJ (2020)
32. Babaie, M., Sharifzadeh, M., Mehrasa, M., Al-Haddad, K.: Optimized based algorithm first order sliding mode control for grid-connected packed E-cell (PEC) inverter. In: 2019 IEEE Energy Conversion Congress and Exposition (ECCE), pp. 2269–2273. IEEE, Piscataway, NJ (2019)
33. Sebaaly, F., Sharifzadeh, M., Kanaan, H.Y., Al-Haddad, K.: Multilevel switching-mode operation of finite-set model predictive control for grid-connected packed E-cell inverter. *IEEE Trans. Ind. Electron.* 68(8), 6992–7001 (2021)
34. Mehrasa, M., Babaie, M., Sharifzadeh, M., Al-Haddad, K.: An input-output feedback linearization control method synthesized by artificial neural network for grid-tied packed E-cell inverter. *IEEE Trans. Ind. Appl.* 57(3), 3131–3142 (2021)
35. Parvez, M., Elias, M.F.M., Rahim, N.A., Blaabjerg, F., Abbott, D., Al-Sarawi, S.F.: Comparative study of discrete PI and PR controls for single-phase UPS inverter. *IEEE Access.* 8, 45584–45595 (2020)
36. Çelik, D.: Lyapunov based harmonic compensation and charging with three phase shunt active power filter in electrical vehicle applications. *Int. J. Electr. Power Energy Syst.* 136, 107564 (2022)
37. Komurcugil, H., Kukrer O.: Lyapunov-based control strategy for power-factor preregulators. *IEEE Trans Circuits Syst I: Fundam Theory Appl* 50(9), 1226–1229 (2003)
38. Sefa, I., Ozdemir, S., Komurcugil, H., Altin N.: Comparative study on Lyapunov-function-based control schemes for single-phase grid-connected voltage-source inverter with LCL filter. *IET Renewable Power Gener.* 11(11), 1473–1482 (2017)
39. Ounejjar, Y., Al-Haddad, K., Dessaint, L.A.: A novel six-band hysteresis control for the packed U cells seven-level converter: experimental validation. *IEEE Trans. Ind. Electron.* 59(10), 3808–3816 (2012)
40. Verma, A.K., Subramanian, C., Jarial, R.K., Roncero-Sánchez, P., Rao, U.M.: A robust Lyapunov's demodulator for tracking of single-/three-phase grid voltage variables. *IEEE Trans. Instrum. Meas.* 70, 1–11 (2021)
41. Verma, A.K., Subramanian, C., Jarial, R.K.: An error demodulation technique for single-phase grid synchronization/LVRT applications. *IEEE Syst. J.* 16(2), 2261–2264 (2022)
42. Ahmed, H., Salgado, I., Chairez, I., Benbouzid, M.: Robust gradient estimator for unknown frequency estimation in noisy environment: application to grid-synchronization. *IEEE Access.* 8, 70693–70702 (2020).
43. Ahmed, H., Benbouzid, M.: Demodulation type single-phase PLL with DC offset rejection. *Electron. Lett.* 56(7), 344–347 (2020)
44. Ioannou, P.A., Sun, J.: *Robust Adaptive Control*, vol. 1. PTR Prentice-Hall, Upper Saddle River, NJ (1996)
45. Ahmed, H., Benbouzid, M.: Gradient estimator-based amplitude estimation for dynamic mode atomic force microscopy: Small-signal modeling and tuning. *Sensors* 20(9), 2703 (2020)
46. Ahmed, H., Biricik, S., Komurcugil, H., Benbouzid, M.: Enhanced quasi type-1 PLL-based multi-functional control of single-phase dynamic voltage restorer. *Appl. Sci.* 12(1), 146 (2021).
47. Bagheri, F., Komurcugil, H., Kukrer, O., Guler, N., Bayhan, S.: Multi-input multi-output-based sliding-mode controller for single-phase quasi-Z-source inverters. *IEEE Trans. Ind. Electron.* 67(8), 6439–6449 (2020)
48. Ahmed, H., Çelik, D.: Sliding mode based adaptive linear neuron proportional resonant control of Vienna rectifier for performance improvement of electric vehicle charging system. *J. Power Sources* 542, 231788 (2022)
49. Meral, M.E., Çelik, D.: Comparison of SRF/PI-and STRF/PR-based power controllers for grid-tied distributed generation systems. *Electr. Eng.* 100(2), 633–643 (2018)
50. Meral, M.E., Çelik, D.: A comprehensive survey on control strategies of distributed generation power systems under normal and abnormal conditions. *Annual Rev. Control* 47, 112–132 (2019)

How to cite this article: Biricik, S., Komurcugil, H., Ahmed, H., Sharifzadeh, M., Mehrasa, M., Al-Haddad, K.: Proportional-resonant based control strategy for grid-connected packed-E cell inverters with Lyapunov filter-based PLL. *IET Gener. Transm. Distrib.* 1–10 (2022). <https://doi.org/10.1049/gtd2.12607>